

# A Hybrid GNSS/RSSI Localization Framework for Precision Tractor Navigation: System Evaluation and Analysis

**Anandakumar Haldorai**

Centre for Future Networks and Digital Twin, Sri Eshwar College of Engineering, Coimbatore, Tamil Nadu, India.  
anandakumar.h@sece.ac.in

**Evelyn Sharma**

University of North Dakota, Grand Forks, ND 58202, United States.  
sharmaind5450@hotmail.com

## Article Info

Journal of Smart and Sustainable Farming  
<https://www.ansispublications.com/journals/jssf/jssf.html>

Received 25 September 2025  
Revised from 10 November 2025  
Accepted 30 November 2025  
Available online 08 December 2025  
**Published by Ansis Publications.**

© The Author(s), 2025.

<https://doi.org/10.64026/JSSF/2025022>

## Corresponding author(s):

Anandakumar Haldorai, Centre for Future Networks and Digital Twin, Sri Eshwar College of Engineering, Coimbatore, Tamil Nadu, India.  
Email: anandakumar.h@sece.ac.in

This article is an open access article distributed under the terms and conditions of the Creative Commons Attribution (CC BY) license (<https://creativecommons.org/licenses/by/4.0/>).

---

**Abstract** – Off-road tractor automation needs navigation technology. In that regard, this study discusses a hybrid location-navigation model, which integrates RSSI and GNSS measurements. Two GNSS-enabled DGNS RTK modules were mounted to a User Portable Device (UPD) alongside a configuration of fixed position wireless routers to measure the RSSI to/from the UPD. The system was tested through various static, dynamic, and real-world scenarios to benchmark the localization capability of the system using a range of available data. The results indicated the DGNS receiver improved localization to an order of a meter and a min-max based algorithm was shown to be superior to the traditional trilateration method. Various hypothesis to determine signal loss of the model RSSI further improved RSSI based localization and demonstrated system flexibility.

**Keywords** – Hybrid Localization System, GNSS, RTK-DGNSS, Received Signal Strength Indication (RSSI), Autonomous Navigation, Off-Road Tractor, Positioning Accuracy.

## I. INTRODUCTION

In the past decade, numerous localization strategies for autonomous vehicles have been developed. A thorough examination of the contemporary advancements in the three predominant localization methodologies; (1) GNSS-IMU fusion, (2) Simultaneous Localization and Mapping (SLAM), and (3) a priori map-based localization, along with their applicability for automated driving, is available in [1]. All localization strategies share the necessity of demonstrating their efficacy for the localization of autonomous vehicles through a validated ground-truth dataset.

The expansion of AI and other linked computer technologies has made location-based services integral to daily life. The Global Navigation Satellite System (GNSS) has achieved sub-meter positioning accuracy, allowing enhanced location services, and is a well-established positioning system for outdoor environments. In unobstructed areas, GNSSs provide high-precision PNT (positioning, navigation, and timing) abilities, resulting in their significant application in various fields such as precision surveillance and smart transportation. Contrarily, their efficacy reduced in severe settings, since signals are typically impacted by factors like reflection, refraction, and buildings [2].

Precise localization offered by the global navigation satellite system (GNSS) encompasses several location-based applications. Examples include surveying, precision agriculture, precision construction machinery, automated drone navigation, advanced driver assistance systems, monitoring of crustal deformation, marine civil engineering, personal



applications in the next years. Traditional GNSS receivers are mostly used in open-sky circumstances because to their technical constraints. Nonetheless, the use of advanced algorithms and enhanced hardware technology enables GNSS to function in almost all environments, with indoor positioning being a significant problem for contemporary GNSS technology.

From the standpoint of a user segment (i.e., the receiver), as described by Fernandez-Prades, Lo Presti, and Falletti [4], the expansion of GNSS-based applications across many domains has resulted in a diversification of application-specific requirements to get the appropriate quality of service. A prevalent and steadily rising need is the combination of precision with prolonged continuity. To get the highest levels of precision, carrier phase location must be emphasized. In the early 1980s, accuracy levels of sub-decimeter precision were shown, first transforming geodesy and subsequently impacting surveying and machine control. At now, carrier phase placement has become more prevalent due to advancements in more economical user equipment and services. For example, augmentation systems using reference station networks provide the precise adjustments necessary to produce the most accurate results. Conversely, robust measurement processing techniques have been devised to estimate and resolve carrier phase ambiguities.

As shown in [5], the Differential Global Navigation Satellite System (DGNSS) idea was established in the 1980s. DGNSS mitigates measurement inaccuracies by using adjustments or raw data derived from one or many reference stations. GNSS errors exhibit spatial correlation, and corrections from reference stations eliminate all satellite clock mistakes, the majority of orbital errors, and most ionospheric and tropospheric errors on the user end. The location precision of the DGNSS user may be enhanced to between 1 m and 2 m, which is enough for several applications. In intelligent transportation systems, DGNSS is combined with other sensors to improve accuracy and reliability; hence, the installation of a specialized DGNSS unit is necessary for vehicle control and safety systems.

The DGNSS positional inaccuracy increases with the distance separating the reference station from the user receiver. The degradation with distance is mostly attributed to the de-correlated error of the ionosphere, which may be alleviated by the use of ionospheric gradients. Be aware that receiver-related mistakes, such as multipath faults, cannot be mitigated by corrections. Sakpere, Oshin, and Mlitwa [6] indicate that multipath errors may be alleviated by the use of inertial navigation systems/computer vision, cooperative positioning, and three-dimensional mapping.

#### *RSSI Localization Methods*

Sensor node localization is a fundamental component in different WSN (wireless sensor network) applications, such as environmental monitoring, target surveillance, disaster management, and rescue operations. The accuracy of localization approach is fundamental for the effectiveness of localization procedures. RSSI-oriented localization approaches represent economical and direct approaches, which depend on the surveillance of receive signal strength indicators during the calculation of distances.

Over the past few decades, several methodologies have been devised to provide effective indoor localization systems. An optimal system would operate effectively in various contexts and accurately monitor a substantial number of targets with minimum mistake. Various comparisons among prevailing technologies have been done in literature to ascertain suitable wireless technologies used for indoor localization.

Comparisons between Wi-Fi and BLE is indicated in [7] when operating on Android smartphones. Most experiments were done using the trilateration method in both indoor and outdoor environments. In the study, testing integrated both non-LoS (non-Line of Sight) and LoS (Line of Sight) that were evaluated alongside propagation features to effectively determine the optimal technology for localization models. RSSI recordings were employed in concurrent with lognormal attenuation framework in order to ascertain node distances.

Their results showed that BLE achieved higher accuracy compared to Wi-Fi when it comes to accurate location. BLE propagation models showed high correlation between RSSI distances and values compared to Wi-Fi, resulting in a model with improved accuracy. Even though energy consumption of various technologies was recorded in the study, no particular energy dataset for employed tools was captured.

#### *Hybrid Positioning Models in Off-Road Ecosystems*

Islam, Nabi, and Ball [8] provide a description of autonomous driving in off-road ecosystems in different possibilities. These systems provide different applications and possibilities, such as forestry monitoring, mining, planetary exploration, and search and rescue operations. In contrast to urban and controlled areas, off-road settings do not provide a discernible trail or useful landmark to facilitate autonomous navigation. Furthermore, the driving area is irregular and inconsistent. Driving on various terrains demonstrates distinct behaviors. In untamed terrain, the user must assess terrain traversability and devise an optimum, terrain-aware route accordingly. Traversability analysis is the assessment of the challenges associated with navigating terrain for an off-road ground vehicle.

Recently, Papadakis [9] precisely delineated terrain position analysis and examined its most recent methodologies in unstructured contexts. Terrain traversability study assesses the challenges a ground vehicle may have while navigating a certain area of terrain. In contrast to obstacle evasion, an obstacle may not always be present in ground-mobility analysis. It assists the robot in making trade-offs between two distinct unencumbered pathways.

Kleiner and Dornhege [10] introduced an innovative method for instant topography that tackles the localization drift issue in multi-limbed robots. The grid-oriented topographic map is a stochastic evaluation of the topography. Every grid cell contains a projected elevation along with its lower and upper confidence boundaries. Chen et al. [11] used the topographic

map and proposed a model for devising an efficient and safe trajectory for multi-limbed robot on unstructured and rugged terrain. Geometric surface attributes are obtained from the elevation data included inside every grid cell. Therefore, a mobility score is calculated from these features and recorded in a mobility cost mapping.

Meng et al. [12] expanded upon the elevation mapping technique and adopted the concept of computing traversability costs based on terrain geometry attributes. In contrast to the aforementioned studies, we are examining not only the geometric aspects of the landscape but also its many varieties. The mobility assessing paradigm is augmented by including vision-oriented semantic dissection of the environmental landscape. A unique method is given to use both semantic and geometrical data.

Consequently, Borges et al. [13] can identify the kinds of terrain in advance and represent them on the mobility cost mapping as well. The robot may strategize a route based on several terrain features in its vicinity, such as avoiding puddles or favoring grassy areas.

### III. MATERIALS AND METHODS

#### Experimental Setup

This experiment tested a hybrid system using GNSS and RSSI. User portable devices (UPD) had two types of satellite receivers. One was an internal GNSS receiver and the other was an external DGNSS receiver. This latter receiver could receive Real-Time Kinematic (RTK) correction signals. The internal GNSS receiver was basic and only listened to satellite signals, but the DGNSS receiver was RTK with a multi-constellation antenna system. The specifications of both modules are described in **Table 1**.

**Table 1.** GNSS Modules Characteristics

Parameter	Internal GNSS Receiver	External DGNSS Receiver
Positioning Technique	Standard GNSS	RTK-DGNSS
Typical Horizontal Accuracy	0.5–2 m	2–4 cm
Update Rate	1 Hz	5–10 Hz
Antenna Type	Embedded Patch	External Survey-Grade

Three wireless routers served as fixed-position Anchor Points at known ground-truth coordinates that formed a non-degenerate triangle for the purposes of trilateration and minimax localization algorithms. These operated on a 2.4 GHz wireless channel and transmitted beacons at regular intervals. Distances between routers were selected to mitigate collinearity and improve overall geometric dilution of precision. An autonomous off-road tractor equipped with a RTK capable rover receiver during the tractor was the mounted on a mast to ensure that there was a clear interpretation of the sky throughout the experiment. This setup maximized satellite constellation geometry while minimizing multipathing throughout the experiment. **Fig. 2** presents a simplified view of the setup.

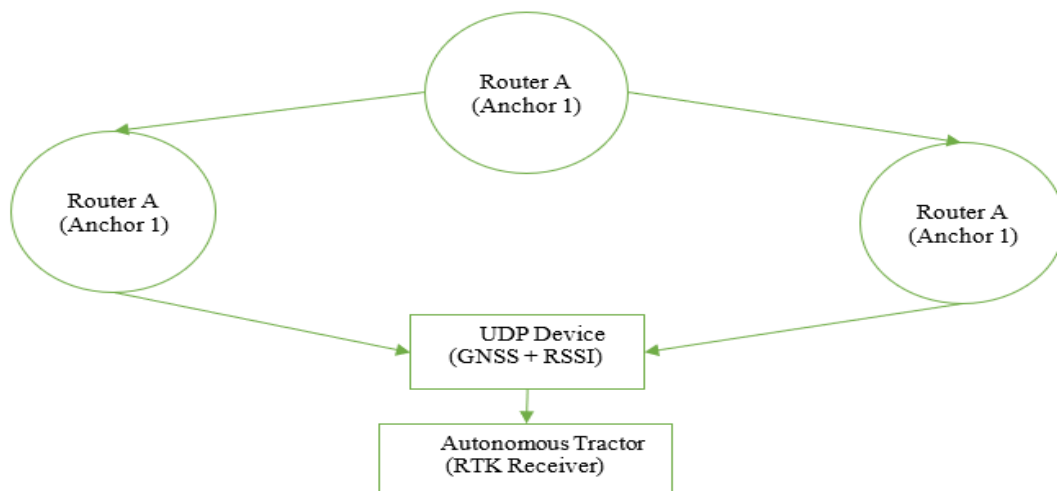


**Fig 2.** Description of Experimental Layout.

**Fig. 2** shows how the UPD, the routers, and the autonomous tractor are positioned with respect to one another. It shows how all the anchor points and receivers used in the test were able to see each other.

#### Test Procedures

The tests consisted of static tests, straight-line traversal tests, dynamic tests, channel model dynamic tests, and field tests with the tractor. Each of these tests was designed with systematic steps to maintain the same process and limit the potential for the introduction of measurement bias.

During static position testing of the position tracking recorders, the UPD was stationary. Data was then logged from the modules for one-, two-, three-, four-, and five-minute increments. These tests with the mobile UPD allowed the calculation of the standard deviation (SD) within an arbitrary east/north coordinate system over several different time frames. These values were used to assess the relationship between the length of the time window (in dwell time) and the accuracy of the system.

Push testing was conducted over a direct path with a distance of 20 m between two ground truth coordinates. The UPD was moved over these coordinates in an even constant step. This created a northing/easting coordinate set for both modules of the GNSS. The divergence from the straight line was then measured. The divergence from the true straight line was measured by using long-tail error models. The straight line, if it is defined by two points, may be parametrically obtained using Eq. (1).

$$L(t) = \begin{bmatrix} x_0 + vt \\ y_0 + wt \end{bmatrix}, 0 \leq t \leq T \quad (1)$$

and the GNSS measurements are computed using Eq. (2).

$$P_i = \begin{bmatrix} x_i \\ y_i \end{bmatrix}, \quad (2)$$

then the instantaneous deviation is expressed using Eq. (3).

$$\delta_i = \frac{|(y_T - y_0)(x_0 - x_i) - (x_T - x_0)(y_0 - y_i)|}{\sqrt{(y_T - y_0)^2 + (x_T - x_0)^2}} \quad (3)$$

In the channel modeling tests, an RSSI measurement was taken every meter from the router from 1m to 50m, with the user standing in one of five cardinal directions at each measurement (facing: forwards, backwards, or one of 3 equidistant angle rotations from the router). The RSSI values recorded, were then processed using Eq. (4) to find the best fitting equation for the long-tail path loss.

$$P_r(d) = P_t + G_t + G_r - (K + 20\log_{10}(d_{km}) + 20\log_{10}(f_{MHz})), \quad (4)$$

Where  $P_r(d)$  is the received power,  $d_{km}$  is distance in kilometers, and  $k$  is an optimized parameter.

Field-based localization tests with the autonomous tractor consisted of five complete circuits of the defined paths. Cross-track errors were calculated using Eq. (5) with the long-tail RMS model from the GNSS readings of the RTK receiver.

$$RMS_{CT} = \sqrt{\frac{1}{N} \sum_{i=1}^N (e_i^2)}, \quad (5)$$

where  $e_i$  denotes the lateral deviation from the planned path.

#### Data Processing and Analysis Techniques

Analyzing data included statistical calculations, trajectory reconstruction, error modeling, and curve fitting. To keep uniformity in distance calculations, all coordinates were processed in the UTM projection. Eq. (6) was used for easting and northing SD computations.

$$\sigma = \sqrt{\frac{1}{N-1} \sum_{i=1}^N (x_i - \bar{x})^2} \quad (6)$$

To assess GNSS drift while performing static tests, the variance for different dwell intervals was calculated using Eq. (7).

$$\text{Var}(t) = \frac{1}{N} \sum_{i=1}^N ((x_i - x_0)^2 + (y_i - y_0)^2), \quad (7)$$

which takes into account radial offsets concerning the actual mean point.

Applying Free Space Loss (FSL) with the constant  $K$  throughout the propagation channel model fitting involved minimization of mean square error (MSE) to be calculated using the Solver tool from Microsoft Excel, in Eq. (8).

$$\text{MSE} = \frac{1}{M} \sum_{j=1}^M (P_{r,j}^{\text{measured}} - P_{r,j}^{\text{model}})^2, \quad (8)$$

and produced an optimized  $k = 45.35$  values for distances over 10 meters which fit the empirical data well.

Localization error for both the min-max and classical trilateration algorithms was obtained using the geometric relationships between router anchors. Three anchors trilateration distances were derived using Eq. (9).

$$d_i = 10^{\left(\frac{P_t + G_t + G_r - P_{r,i} - K - 20 \log_{10}(f)}{20}\right)}, \quad (9)$$

and the position estimate  $(x, y)$  is estimated as the solution to an overdetermined system of circle intersection equations, which is then solved using least-squares estimation in Eq. (10).

$$\min_{x,y} \sum_{i=1}^3 \left( \sqrt{(x - x_i)^2 + (y - y_i)^2} - d_i \right)^2 \quad (10)$$

For the min-max localization algorithm, we first derived position estimates using the intersection of axis-aligned bounding boxes defined by the RSSI-based distance thresholds, mathematically described using Eq. (11).

$$x_{\text{est}} = \frac{\max(x_L) + \min(x_U)}{2}, y_{\text{est}} = \frac{\max(y_L) + \min(y_U)}{2} \quad (11)$$

The data from the tractor's navigation system were analyzed to determine the root mean square (RMS) cross-track error, max deviation, and SD for each pass. Resulting data are highlighted in **Table 2**.

**Table 2.** Outputs of Processed Data from Tractor RTK Trials

Metric	Result
RMS cross-track error	2.4 cm
Maximum lateral deviation	< 4 cm
SD between rows	1.43 cm

**Fig. 3** provides a flowchart, which summarizes the data-processing pipeline employed in our study.

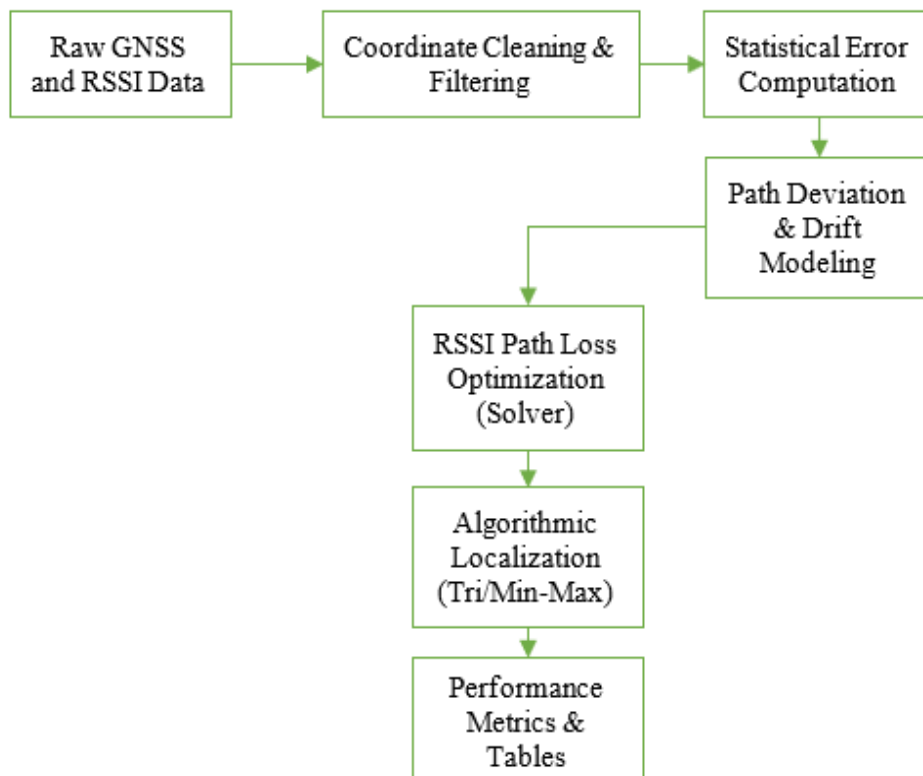


**Fig 3.** Data Analysis Flowchart.

#### IV. RESULTS AND ANALYSIS

This section shows and analyzes the first findings from the smart off-road vehicular localization and UDP assessments. UDP experiments used both RSSI and GNSS localization techniques. Approximately 1500 occurrences were documented in the dynamic and static GNSS assessments, whereas about 800 occurrences were documented in the RSSI evaluations. Out of the 16,690 occurrences computed across 5 iterations of the vehicular test, 610 were employed to assess the accuracy degree. This research gathered more data than other studies; nevertheless, it was restricted to a single producer’s deployment of an RTK-GNSS model.

##### Static GNSS Localization Accuracy Assessment

The findings of the static experiments are provided in **Table 3**. The first row indicates the duration of the agent’s stay at a certain place, whereas each row corresponds to data for an individual receiver. The table presents the SD pairs computed for the northings and eastings coordinates. As coordinates are in the UTM format, all values are calibrated in meters.

**Table 3.** Static Positioning Precision

	1 Minute	3 Minutes	5 Minutes
DGNSS $\Delta[E, N](m)$	[.13,.33]	[.04,.05]	[.03,.04]
GNSS $\Delta[E, N](m)$	[.08,.09]	[.10,.30]	[.05,.30]

**Table 3** presents the positional accuracy achieved with the 2 GNSS components. The UPD achieved an 8 cm and 9 cm precision in easting and northing, respectively, when the exterior DGNSS component was employed for 1 minute. The precision improved with more duration spent at a certain location; for instance, the precision was 3.01 cm in the easting direction and 4.01 cm in the northing direction after 5.01 minutes. The optimal precision attained with the interior GNSS detector was 30 cm in the northing direction and 5 cm in the easting direction after 5 minutes. The DGNSS detector exhibited double the accuracy in the easting coordinate and about quintuple the accuracy in the northing direction compared to the interior GNSS detector.

**Fig. 4a** and **4b** illustrate the occurrence frequency within every positional range, as recorded by the interior GNSS detector during a 5-minute period (300 experiments) for the northing and easting coordinates. All experimented easting sites are confined to a 60 cm range, with nearly 60% of the dimensions situated within a 20.11 cm interval (40 to 60 cm, refer to **Fig. 4a**). All except 1 indicated that northings are confined to a 200 cm range, with almost 75% of the data falling within a 120 cm interval (40 to 160 cm, refer to **Fig. 4b**).

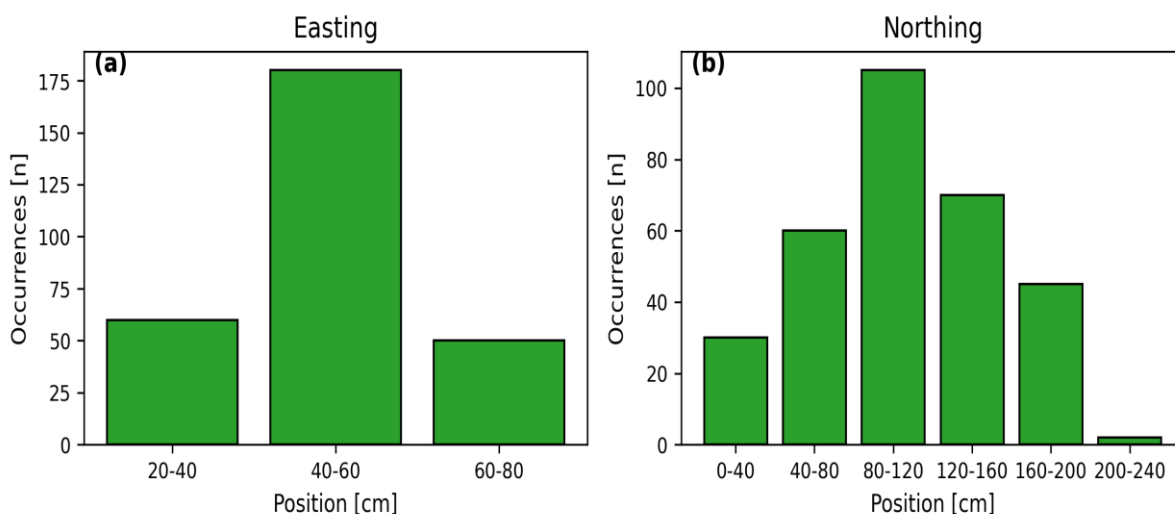


**Fig 4.** Distribution of GNSS (a) Eastings, and (b) Northings.

**Fig. 5a** and **5b** illustrate the frequency of events within every positional range, as recorded by the exterior DGNSS detector during a 5-minute period (300 experiments) for the northings and eastings. All experimented eastings are confined to a 40 cm range, with around 65% of data falling within an interval of 20 cm (20 to 40 cm, refer to **Fig. 5a**). All measured numerical values are calibrated between the initial two ranges (see **Fig. 4a**). The documented northing positions span an interval of 80 cm, with almost 90% of the observations confined to 40.01 cm (300 to 340 cm, refer to **Fig. 5b**).

The findings shown in **Table 3** and **Fig. 4** and **Fig. 5** indicate that both detectors exhibited superior accuracy in easting compared to northing. The impact was more pronounced with the interior GNSS detector, since the disparity between the SD of northings and eastings exceeded that seen with the external DGNSS receiver. Both receivers, however, demonstrated

sub-meter accuracy in all assessments. Furthermore, no correlation was identified between positioning accuracy and the duration spent in a specific site, or at least no correlation was discernible using conventional statistical methods, such as SD.

**Fig. 6** illustrates the findings of the second test series that assessed the discrepancy between the actual and linear trajectories. Both the interior GNSS sensors and the exterior DGNSS trajectories are shown. The traversal of 20 meters between points A and B took 22 seconds, given that there are 22 locations in total. The journey started at the top left and concluded at bottom right, following a southeast to northwest compass trajectory.

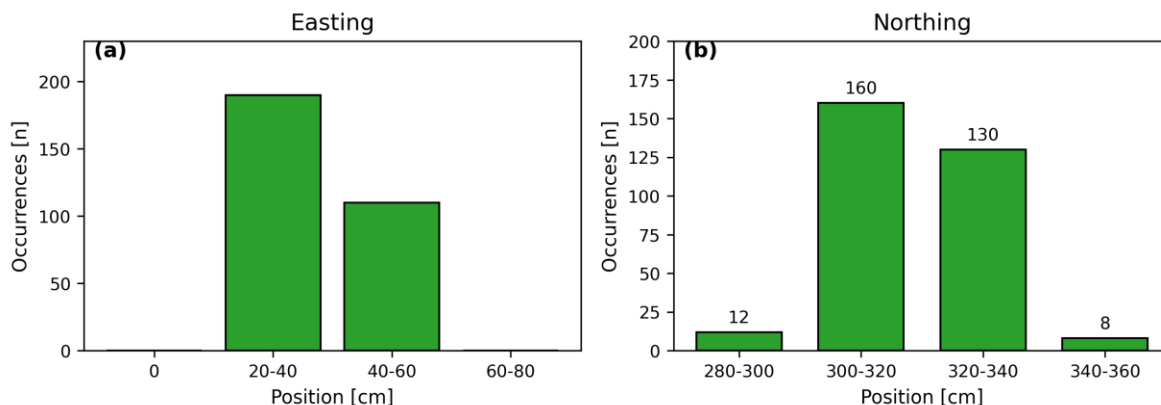


**Fig 5.** Distribution of DGNSS (a) Eastings, and (b) Northings.

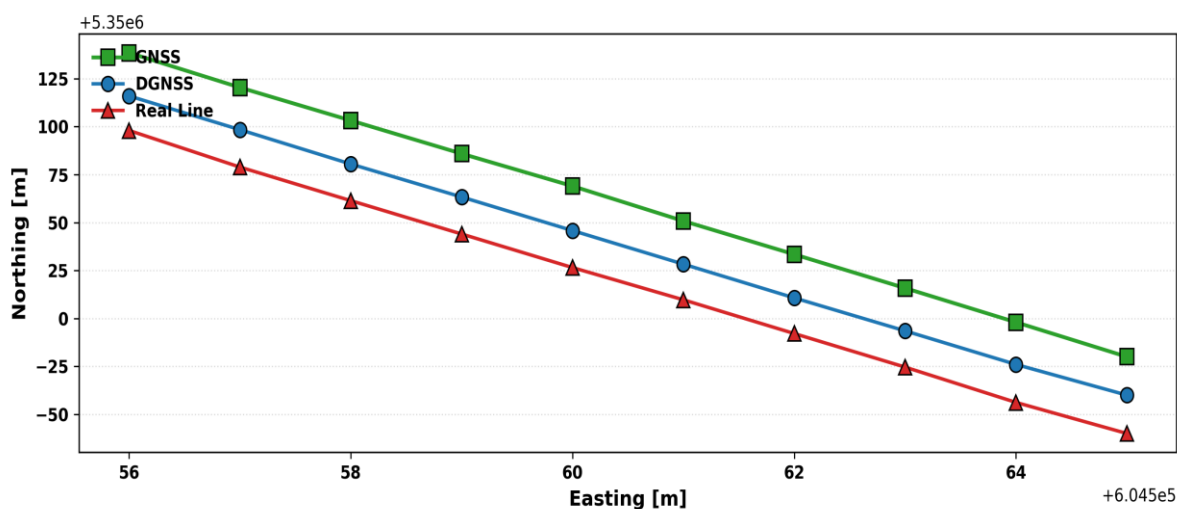


**Fig 6.** Discrepancy Between the Real and Linear Trajectories Derived from DGNSS and GNSS Sensors.

**Fig. 6** (red line) illustrates the linear route. The last two lines relate to the dataset from the chosen detectors. The blue line, signifying the exterior DGNSS detector, shows little deviation from the line, unlike the green line, which denotes the interior GNSS receiver. Additionally, a section of the blue line (between 604,561-604,557 meters) coincides with the parallel line. Nonetheless, there is no convergence between the linear trajectory and GNSS dataset. The findings shown in **Fig. 6** are listed in **Table 4**. **Table 4** represent the two receivers, corresponding to the green and blue lines seen in **Fig. 6**. **Table 4** displays the average nonconformity from the linear trajectory obtained from a series of 22 tests.

**Table 4.** Average Deviations from the Linear Trajectory.

	GNSS	DGNSS
Mean (m)	1.19	0.21

In addition to **Fig. 6**, **Table 4** corroborates that the blue line denoting the DGNSS is much nearer to the optimal trend (exhibiting an average variation of 21 cm) compared to the green line signifying GNSS (that shows a variance of 119 cm). The ideal line and the green line are almost congruent in direction and slope, differing only by an approximate displacement of 2 meters.

*RSSI-Based Localization and Channel Modeling Results*

This section presents the findings recorded from the channel modeling and RSSI localization samples. The gathered test data underwent statistical analysis, and the mean outcomes from the 5 localizations are shown in **Fig. 7** as an element of the

length of the UPD from routers. **Fig. 7** (blue dotted line) represents the mean values of experimental data obtained throughout interval tests. The red line represents the modified route loss modelling, derived from the path loss modelling outlined in [14]. This research evaluated the Walfisch-Ikegami, HATA, and CCIR route loss modeling with the sampling results. We deemed the FSL modeling, outlined in Eq. (12), to be the most appropriate since it allows for the adjustment of parameter K to optimally align with the observed numerical quantity:

$$P_i[\text{dBm}] = P_{T_x} + G_t + G_r - (K + 20 \log_{10}(d_{km}) + 20 \log_{10}(f_{\text{MHz}})) \quad (12)$$

The power of the signal  $P_i$  (in dBm) at node  $i$ , situated  $d_{km}$  from the transmitter, is expressed by Equation (3) as the aggregate of the diffused power  $P_{Tx}$  (in dBm) and the gains of the receiver and the transmitter antennas,  $G_r$  and  $G_t$ , respectively, with the distance  $d_{km}$ , frequency  $f_{\text{MHz}}$ , and a constraint K incorporated. To enhance the route loss model parameter K, we decreased the mean squared error using Excel's Solver tool.  $K = 45.35$  was the outcome of the optimization procedure, in contrast to the 32.45 reported in [15].

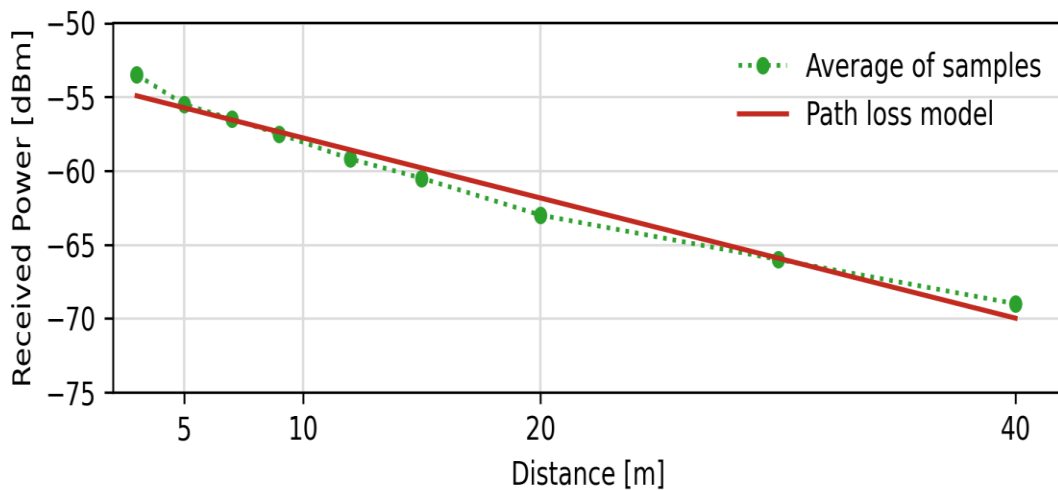


**Fig 7.** Signal Power Levels Sampled for Channel Model.

**Fig. 7** illustrates that, considering all factors, the correlation of the experimental dataset is rather strong. Short distances (under 10 m) between the UPD and router exhibit variances between anticipated and observed values. The hybrid positioning system must nevertheless correct for these inaccuracies, since safety laws stipulate that the operator and the autonomous tractor cannot be more than 10 meters apart. The maintenance requirements of an autonomous tractor may be predicted by using the tractor's characteristics to ascertain the user's present location. **Fig. 8** illustrates the findings of the localization test, demonstrating the variation in localization error based on the user's orientation.

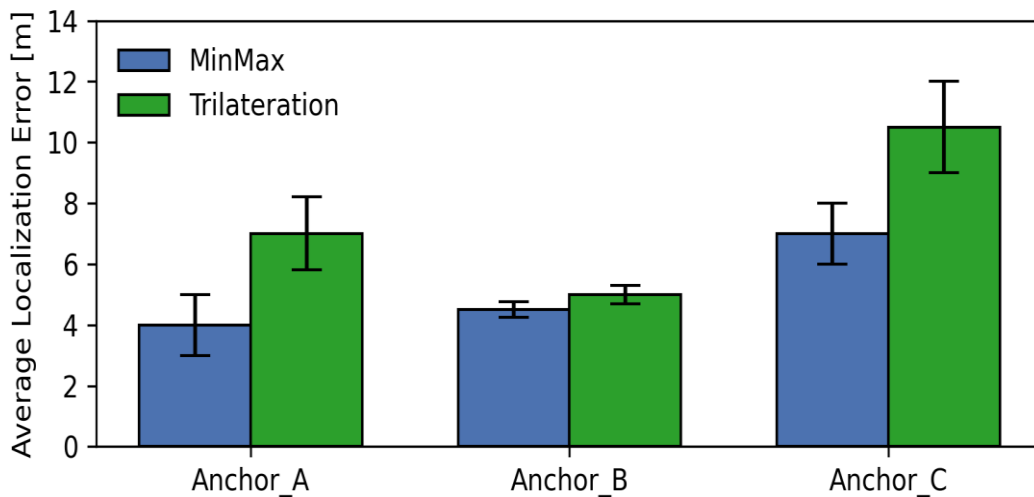


**Fig 8.** Localization Error.

Routers A, B, and C are designated as Anchors A, B, and C, respectively, in **Fig. 2**. Every bar displays the standard nonconformity to measurements, while the figures on the bars indicate the averages of the gathered data. The error determined by the trilateration method is shown by the red bars, whilst the min-max algorithm is depicted by the blue bars. **Fig. 8** illustrates that, in comparison to the traditional trilateration strategy, the min-max algorithm produces high results with minimal errors.

In optimum states, the min-max algorithmic error is 4 meters. However, in various adverse states, it is recorded at 7 meters. The trilateration method attains a localization error not exceeding 10 meters, with a minimum of 4.5 meters. The min-max method demonstrates superior performance in localization using wireless connections by centering the user inside the region defined by horizontal and vertical lines.

*RTK-GNSS Performance in Autonomous Tractor Field Trials*

**Table 5** displays the errors resulting from the off-road tractor’s GNSS receiver employing RTK-GNSS modification signals, together with their RMS and standardized error values. The rover receiver exhibited 2.51 cm of straight precision and 3.71 cm of vertical precision during constant real-time operation. The RTK approach can determine the sensor’s location with an accuracy of a few millimeters; so, this degree of precision was anticipated [16]. The RTK corrective signal system’s mean RMS cross-track error of 2.41 cm indicates that the trajectories were mostly linear, as anticipated from the automated tractor.

The inaccuracy between the rows exhibited a consistent standard deviation; the RTK method produced a mean value of 1.43 cm. The controller of the tractor accurately adhered to every straight line, exhibiting a deviation of under 3.5 cm; concurrently, the lateral location error of the vehicle using the RTK approach did not exceed 4 cm. This indicates that completely autonomous tractors may be employed for robotic precision agriculture across various scenarios, including targeted weed management in wide-ranging crops, differential fertilizer application in diverse vineyards and orchards utilizing suitable equipment, and tailoring these applications based on yield maps [17].

**Table 5.** Data Pertaining to GNSS Receivers on Mobile Automated Tractor Using RTK Modification Signals

Row	S.D.	RMS	Measurement
1	2.10	2.71	122
2	1.52	3.36	122
3	0.87	1.36	122
4	1.61	2.93	122
5	1.05	1.65	122
All Rows	1.43	2.40	610.00

The placement of the GNSS antennae on the unmanned tractor afforded an unobstructed orientation of the whole sky. This optimized the opportunity for achieving favorable satellite calibration, while ensuring consistent RTK-GPS quality for data computations.

V. CONCLUSION

This study has shown that GNSS and RSSI positioning systems are accurate particularly when using RTK technology for modulation as opposed to using the internal GNSS receiver alone. The system showed additional improvements when using the min-max technique as opposed to traditional trilateration for positioning. The changes to the loss model used for RSSI communication were well-suited for the actual received signal strength. The results for this study for the hybrid system are such that using both RTK and RSSI has the potential to significantly enhance the systems used in agricultural technologies and other autonomous systems.

**CRedit Author Statement**

The authors confirm contribution to the paper as follows:

**Conceptualization:** Anandakumar Haldorai and Evelyn Sharma; **Methodology:** Anandakumar Haldorai; **Software:** Anandakumar Haldorai; **Data Curation:** Evelyn Sharma; **Writing- Original Draft Preparation:** Anandakumar Haldorai; **Visualization:** Evelyn Sharma; **Investigation:** Anandakumar Haldorai; **Supervision:** Anandakumar Haldorai; **Validation:** Anandakumar Haldorai and Evelyn Sharma; **Writing- Reviewing and Editing:** Anandakumar Haldorai and Evelyn Sharma; All authors reviewed the results and approved the final version of the manuscript.

**Data Availability**

The datasets generated and/or analyzed during the current study are available from the corresponding author on reasonable request.

**Conflicts of Interests**

The authors declare no conflict of interest.

**Funding**

No funding agency is associated with this research.

## Competing Interests

There are no competing interests.

## References

- [1]. J. Fayyad, M. A. Jaradat, D. Gruyer, and H. Najjaran, "Deep Learning Sensor Fusion for Autonomous Vehicle Perception and Localization: A review," *Sensors*, vol. 20, no. 15, p. 4220, Jul. 2020, doi: 10.3390/s20154220.
- [2]. M. A. U. Haq et al., "A review on lighting control technologies in commercial buildings, their performance and affecting factors," *Renewable and Sustainable Energy Reviews*, vol. 33, pp. 268–279, Mar. 2014, doi: 10.1016/j.rser.2014.01.090.
- [3]. S. Madry, *Global Navigation satellite Systems and their applications*. 2024. doi: 10.1007/978-3-031-74488-4.
- [4]. C. Fernandez-Prades, L. Lo Presti, and E. Falletti, "Satellite radiolocalization From GPS to GNSS and beyond: Novel technologies and Applications for civil Mass market," *Proceedings of the IEEE*, vol. 99, no. 11, pp. 1882–1904, Jul. 2011, doi: 10.1109/jproc.2011.2158032.
- [5]. W. Lechner and S. Baumann, "Global navigation satellite systems," *Computers and Electronics in Agriculture*, vol. 25, no. 1–2, pp. 67–85, Jan. 2000, doi: 10.1016/s0168-1699(99)00056-3.
- [6]. W. Sakpere, M. A. Oshin, and N. B. Mlitwa, "A State-of-the-Art survey of indoor positioning and navigation systems and technologies," *South African Computer Journal*, vol. 29, no. 3, Dec. 2017, doi: 10.18489/sacj.v29i3.452.
- [7]. J. F. Ensworth and M. S. Reynolds, "BLE-Backscatter: Ultralow-Power IoT nodes compatible with Bluetooth 4.0 low energy (BLE) smartphones and tablets," *IEEE Transactions on Microwave Theory and Techniques*, vol. 65, no. 9, pp. 3360–3368, Apr. 2017, doi: 10.1109/tmtt.2017.2687866.
- [8]. F. Islam, M. M. Nabi, and J. E. Ball, "Off-Road Detection Analysis for Autonomous Ground Vehicles: a review," *Sensors*, vol. 22, no. 21, p. 8463, Nov. 2022, doi: 10.3390/s22218463.
- [9]. P. Papadakis, "Terrain traversability analysis methods for unmanned ground vehicles: A survey," *Engineering Applications of Artificial Intelligence*, vol. 26, no. 4, pp. 1373–1385, Feb. 2013, doi: 10.1016/j.engappai.2013.01.006.
- [10]. A. Kleiner and C. Dornhege, "Real-time localization and elevation mapping within urban search and rescue scenarios," *Journal of Field Robotics*, vol. 24, no. 8–9, pp. 723–745, Aug. 2007, doi: 10.1002/rob.20208.
- [11]. Y. Chen et al., "Learning autonomous and safe quadruped traversal of complex terrains using Multi-Layer elevation maps," *IEEE Robotics and Automation Letters*, vol. 10, no. 10, pp. 9606–9613, Aug. 2025, doi: 10.1109/lra.2025.3595814.
- [12]. X. Meng, Z. Cao, S. Liang, L. Pang, S. Wang, and C. Zhou, "A terrain description method for traversability analysis based on elevation grid map," *International Journal of Advanced Robotic Systems*, vol. 15, no. 1, Jan. 2018, doi: 10.1177/1729881417751530.
- [13]. P. Borges et al., "A Survey on Terrain traversability Analysis for Autonomous ground vehicles: methods, sensors, and challenges," *Field Robotics*, vol. 2, pp. 1567–1627, Jul. 2022, doi: 10.55417/fr.2022049.
- [14]. S. Kurt and B. Tavli, "Path-Loss Modeling for Wireless Sensor Networks: A review of models and comparative evaluations," *IEEE Antennas and Propagation Magazine*, vol. 59, no. 1, pp. 18–37, Jan. 2017, doi: 10.1109/map.2016.2630035.
- [15]. K. O. Olatunji, S. O. Oladipo, D. M. Madyira, and Y. Sun, "Performance evaluation of different clustering techniques and parameters of hybrid PSO- and GA-ANFIS on optimization and prediction of biomethane yield of Alkali-Pretreated Groundnut shells," *Waste and Biomass Valorization*, vol. 16, no. 1, pp. 423–440, Aug. 2024, doi: 10.1007/s12649-024-02674-2.
- [16]. S. Touati et al., "Performance analysis of steel W18CR4V grinding using RSM, DNN-GA, KNN, LM, DT, SVM models, and optimization via desirability function and MOGWO," *Heliyon*, vol. 11, no. 4, p. e42640, Feb. 2025, doi: 10.1016/j.heliyon.2025.e42640.
- [17]. M. Padhiary, R. Kumar, and L. N. Sethi, "Navigating the Future of Agriculture: A Comprehensive review of Automatic All-Terrain Vehicles in Precision Farming," *Journal of the Institution of Engineers (India) Series A*, vol. 105, no. 3, pp. 767–782, Jun. 2024, doi: 10.1007/s40030-024-00816-2.

**Publisher's note:** The publisher remains neutral with regard to jurisdictional claims in published maps and institutional affiliations. The content is solely the responsibility of the authors and does not necessarily reflect the views of the publisher.

ISSN: 3104-4654